Lab 5: Near Infrared Observations of T Tau System

Pierre Christian*

November 16th 2010

Abstract

The T Tauri system, comprising of T Tau N, T Tau Sa, and T Tau Sb, is a three star system in the constellation Taurus. In this lab we used the adaptive optics system of Keck and VLT to peer into this system in the near infrared regime. Using datasets spanning from 2002 to 2009, we were able to monitor the changes of the distances separating these stars. Furthermore, we were also able to measure the magnitudes of T Tau Sa and T Tau Sb as a function of time. From said measurement and the aid of a color-color diagram, we were able to confirm their statuses as pre-mainsequence protostars. By measuring their magnitudes over time, we also confirmed that they are indeed variable stars.

1 Introduction

The T Tau system, comprising of T Tau N, T Tau Sa, and T Tau Sb, is a gravitationally bound system of at least three stars. This system is of interest because it hosts the prototypical namesake for young, pre-mainsequence variable stars called T Tauri stars. Under an optical filter, only T Tau N is visible, with T Tau Sa and T Tau Sb clouded behind a veil of dust. All three components of the system, however, can be seen in the near-infrared.

*University of California, Berkeley

Another challenge in observing this system, which was circumvented only recently, is that the Earth's atmosphere rendered distinguishing these three stars apart impossible. With the use of adaptive optics, we are capable to take images at close to their diffraction-limited resolutions, enabling us to discern the separations between these three stars.

2 Equipments

2.1 Keck

The Keck telescopes are two reflecting telescopes situated about the summit of Mauna Kea in Hawai'i. Each of their primary mirrors is a hexagonal mirror measuring 11 meters across composed of multiple smaller hexagonal mirrors. In this lab, we are to use one of them equiped with the near-infrared camera NIRC-2 (Near Infrared Camera-2). In the configuration used in this lab, the NIRC-2 detector is broken into an array of 1024×1024 pixels, with $0.01 \pm 5 \times 10^{-5}$ arcseconds/pixel plate scale. Furthermore, the gain of this detector is 4 electron/count.

2.2 Very Large Telescope

The Very Large Telescope (VLT) is an interferometric system of four separate reflecting telescopes each with 8.2 m aperture. This lab utilizes the VLT's NACO (Nasmyth Adaptive Optics System and Coude Near Infrared Camera) to take near infrared observations of the T Tauri system. In our configuration, the NACO's near-infrared detector is broken into an array of 1024×1024 pixels with $13.25 \pm 6.6 \times 10^{-3}$ miliarcseconds/pixel plate scale. This time, the gain of the detector is 11 electron/count.

2.3 Adaptive Optics

According to Fourier optical analysis, the resolution limit of a telescope of diameter D observing at a wavelength λ is given by:

$$\theta_{min} = \frac{\lambda}{D} \tag{1}$$

Where θ_{min} denotes the smallest angle (expressed in radians) that the telescope can distinguish. However, in practice atmospheric turbulence limits the resolution of ground based telescope far before it reaches this ideal value.

Adaptive optics is a technique developed to compensate for this atmospheric blurring in real time. It works by taking the flux of a reference beacon (can be a bright star or one artificially made using a bright laser) which is affected by the same atmospheric turbulence as the science target. A wavefront sensor would measure the effects of the atmospheric turbulence on the flux of the reference beacon. This information would be sent to a deformable mirror, which would use it to compensate for the atmospheric turbulence my moving small pistons which physically alter the shape of the mirror. Both Keck and the VLT possessed this system which we would utilize in this lab.

3 Data and Observation

3.1 Observations

We obtained four datasets of the T Tauri system: three Keck NIRC2 datasets taken on December 12 2002, October 20 2008, and December 08 2009, and a VLT NaCo dataset taken on October 11 2006. Due to the brightness of the T Tauri system, each of these images were taken with very short exposure time to avoid saturating the detector pixels. Numerous of these short integration time images were then summed together to form a single coadded image to increase signal to noise ratio.

Our 2002 dataset is a three band observation, with images of the T Tau system in the K_{cont} (centered at 2.27 micron), L' (centered at 3.78 micron), and M_s (centered at 4.67 micron) filters. The K_{cont} images include 400 short integration time images of the T Tau system. These 400 images were summed by 100 each, forming 4 coadded images of 0.053 seconds integration time each. A further 400 short integration time science images were taken for the L' filter and 200 were taken for the M_s filters. Coadding every 100 images gives us 4 coadded T Tau images for the L' filter and 2 for the M_s filter. Due to their single image integration time being less than that of the K_{cont} band, both the L' and M_s coadded science images possessed the effective integration time of only 0.018 seconds each. Furthermore, in order to facilitate fast enough readout time, only a small subset of the entire detector array was used for

each observations. The K_{cont} images only used a 512×512 subsection of the entire 1024×1024 array. Simillary, the L' images used a 256×264 subset, and the M_s images used a mere 128×152 subset of the entire array.

The next two Keck datasets were taken using the BRγ filter (centered around 2.17 μm) making use of the entire 1024×1024 detector array. These 2008 and 2009 datasets consists of 6 and 10 coadded images of the T Tau system respectively. Our 2006 VLT dataset was taken using the K_s filter centered around 2.18 μm. It consists of a further 5 coadded images of the T Tau system.

3.2 Calibration and Corrections

3.2.1 Dark Counts, Sky Noise, and Bias

Thermal excitations can excite electrons on our detector, causing faulty signals to be recorded. In addition to these thermal noise, the sky is also very bright in the near infrared. These sky fluxes would also contaminate our datasets with signals that does not occur due to the fluxes of our science targets. Removal of these noises from our datasets are done using a variety of techniques.

In our 2002 dataset, we were provided with four coadded dark images and a single coadded sky image for each of our filters[1]. In order to compute a master dark frame for every filter, we took the median data number per pixel of the four dark images. Our M_s dark frames were taken with different effective integration times compared to our science images. Theoretically, dark currents increase linearly with time, thereby disallowing us to correct our M_s images with the M_s dark frames. However, in practice, the detector of the NIRC2 is cooled to very low temperatures, resulting to a very low thermal noise. As such, we can neglect the dark counts contributions and the dark frames effectively only measure the bias, a systematic offset of the recorded signals artifically introduced by the detector's manufacturer. By subtracting our dataset with the master dark frames of their corresponding filters, we can correct our data from their bias.

In order to correct for the sky noises, we first need to correct our sky

[1]Dark frames are taken without filters. However, the science images of each filters were taken with different sizes subsection of the entire array. The four dark images per filter here refers to four dark images taken with the subarray sizes corresponding to the three filters.

images for dark, bias, and QE differences by first subtracting the sky images by the dark frames of their respective filters. Afterwards, we flat field the sky images by dividing it with their respective flat-field images. Subtracting these images from the science images of their corresponding filters would effectively removed the sky noise from our dataset. In addition to these corrections, we would also reduce the median of our science images to zero by subtracting them with their medians.

Our 2006, 2008, and 2009 datasets does not include dedicated dark or sky frames. Fortunately, the dark counts, sky noise, and bias contributions on each image can be reasonably approximated by the median of the flat fielded science image[2]. This is because most of the pixels in our science images are exposed to an empty patch of sky. The median, therefore, would give us a representative data number of a pixel with nothing but dark current, bias, and sky noise contributing to its recorded signal. Ridding these noises can therefore be done by subtracting our science images by their medians. It should be noted, however, that by using this method we made the assumetion that the dark currents, sky noise, and bias are spatially uniform. Again, we would afterwards reduce the median of our science images to zero by subtracting them with their medians.

3.2.2 Flat Fielding

In order to correct for the quantum efficiency differences between the pixels of our detectors, we have to perform flat fielding on our science images. In practice, this is done by first taking an image of a bright uniform source to serve as a map of the quantum efficiencies of the detector's pixels, and then dividing our science image with this map.

Our 2002 dataset possessed three dome flat-field images taken in the K' band. These images were taken with the dome closed and illuminated by a lamp acting as the bright uniform source. We also possess three images taken in the K' band with the dome closed and the lamp off. These images can be used to correct our dome flat-fields from dark currents and bias. This is done by first calculating the median of these 3 images per pixel, creating a master dark frame, then subtracting this master dark frame from our dome flat-fields. We then normalize each of the dome flat-field images by dividing it by its median. Afterwards, we can take the median of our 3 dome flat

[2]Flat fielding will be discussed in the next section

fields per pixel to create a master flat field image for the K' band. Since the K' band is centered around the same wavelength as the K_{cont} band, we can use this resulting flat field image to correct our K_{cont} science images from QE variations. We do not have dedicated flat-field images for the M_s and L' filters, so we have to emulate flat-field images using their sky images. This is because the sky images, once corrected for the dark and bias using the dedicated dark frames of its filters, forms a reasonably good approximation of a bright uniform source. We can therefore get twilight flat frames for these two filters by taking their sky, subtracting them with their respective master dark frames, and normalizing them by dividing it with their respective medians. Conveniently, our 2006, 2008, and 2009 datasets came with flat-field images that were already normalized and corrected for dark and bias.

3.3 Theoretical Considerations

3.3.1 Thereotical PSF

The point spread function is the response of our instrument to a point source. Since a star is effectively a point source as seen from the Earth, its image would be a point spread function. In Fourier optics, the perfect PSF for a telescope would be the magnitude of the Fourier transform of the entrace pupil. In a circular filled aperture, the PSF would be the Airy function. On the Keck telescope, since the aperture consists of a large hexagonal primary mirror covered at the center by a smaller hexagonal secondary mirror, our PSF would deviate from this ideal Airy function. For our 2002 dataset, the inscribed circle pupil of the NIRC-2 was used, thereby reducing our aperture into a 9 m filled circle with a 1 m circle hole in the middle due to the presence of the secondary mirror. The FWHM of the resulting theoretical PSF calculated by taking the Fourier transform of this aperture is given in Table 1. In figure form, these theoretical ideal FWHMs are plotted in Figure 2. Overplotted on the figure is the best case scenario of equation (1). As seen in this figure, even with no atmosphere, our resolution limit is still greater than that of equation (1) purely due to the geometry of our telescope's aperture.

K_{cont} (arcseconds)	L' (arcseconds)	M_s (arcseconds)
$0.0704 \pm 5 \times 10^{-5}$	$0.123 \pm 5 \times 10^{-5}$	$0.15 \pm 5 \times 10^{-5}$

Table 1: The Full Width Half Maxes of the theoretical PSF's of the 2002 Keck data. These values were calculated by fitting a gaussian to the theorerical PSF of each of the filters. The errors are due to the uncertainties of the plate scale.

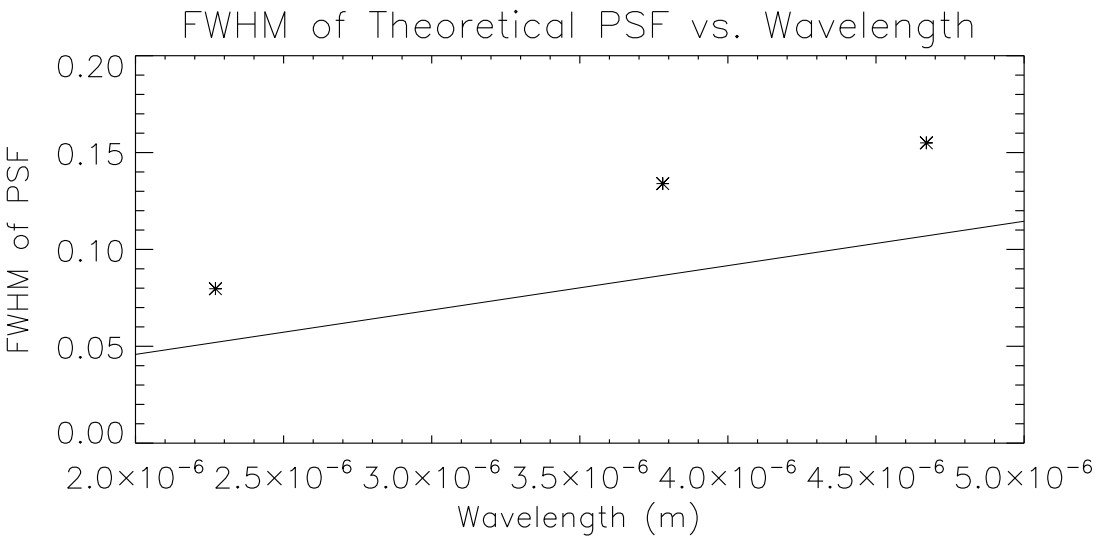

Figure 1: Plot of the FWHMs of the theoretical PSF's of the 2002 Keck data. Overplotted over it is the best case scenario of equation (1). Notice that even our theoretical FWHMs are still greater than that of equation (1), meaning that even with no atmosphere, we would still get a worst resolution than the best case scenario purely due to the geometry of our aperture.

3.3.2 Background Level

Figure 2 shows the intensity of the sky flux versus wavelength. The sky flux values was calculated by taking the median of the bias and dark corrected flat-fielded sky images of the three filters of the 2002 dataset. In order to put all three values on the same footing, we had also divided them by their effective integration times.

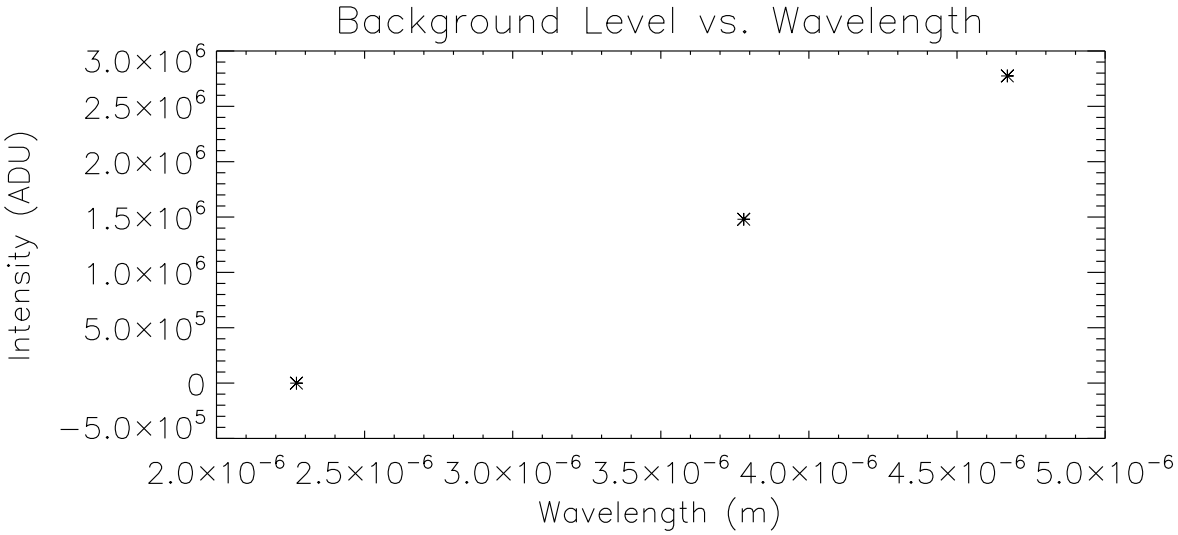

Figure 2: Background intensity versus wavelength of our 2002 dataset. Note that the higher our wavelength, the higher is the background flux. This is because as we increase our wavelength, we are getting closer to the infrared regime. As the Earth thermally radiates in the infrared, the sky is very bright close to the infrared regime.

As seen in this figure, the sky (or background) flux contributions raises very quickly as we increase wavelength. This is due to the earth thermally emitting strongly in the infrared. These emitted lights are reflected back to the ground by the atmosphere, effectively making the sky very bright in the infrared regimes. As such, the closer our filter's wavelengths are to the infrared, the more sky noise we would receive. Furthermore, since the dark currents and bias does not depend on our filter's wavelengths, the sky noise would quickly dominate over them around the infrared regime.

3.4 Relative Astrometry and Photometry

3.4.1 Alignment

The Keck December 12 2002 dataset was taken in vertical mode, where the telescope rotates the sky continuously throughout the observation. As such, the images from this dataset are rotated differently from one another. Before we can perform any spatial alignment, we have to first correct for this rotation differences. Fortunately, the position angles(PA)[3] of each image are recorded in the image header. We can therefore rotate each image by the negative of their PA's to bring them to the same reference rotation frame where North is at the top of the image and East is to the left. In practice, this rotation is done using the IDL built in function ROT. Furthermore, the arbritrary negative sign in our rotation is to match the rotation frames of the other datasets, which were taken in position angle mode, an observation mode that forces the telescope to orient north at the top of the image and East to the left of the image.

The next step is to align each images so that regions around the T Tau system on every images corresponds to the same pixel positions for every images in a single epoch. In order to perform this alignment, first find the approximate pixel position of the center of the bright T Tau N star using IDL's cursor function. We then fit a 2 dimensional gaussian function to the star's flux around its approximate center position using the build in IDL function gauss2dfit. The peak of the gaussian surface would indicate the pixel position of the center of T Tau N. By performing this routine on each images of a single epoch, we would obtain the pixel positions of T Tau N on each of those images. We can then use IDL's shift function to shift each images so that this peak corresponds to the same pixel position on every images in the epoch, thereby effectively aligning the images on the regions around the T Tau system. After this alignment is done, we would then coadd the aligned images by adding them all together and dividing them by the number of images that go into the coaddition in order to improve signal to noise. The resulting images are provided in the Apendix section.

[3]Position angles are defined so that PA=0 points North and PA=90 points East.

3.4.2 Point Spread Function

The FWHMs of the experimental PSFs can be calculated by fitting a gaussian to the star T Tau N on our aligned and reduced images. The FWHM of one of these 2 dimensional gaussians, calculated by taking the average of the standard deviations of the gaussians in the two dimensions and multiplying it by $2\sqrt{2ln2}$, would indicate the FWHM of the experimental PSF of the image. Afterwards, we can convert these pixel gaussians into units of arcseconds or milliarcseconds using the plate scale, $0.01 \pm 5 \times 10^{-5}$ arcsecs/pix and $13.25 \pm 6.6 \times 10^{-3}$ milliarcsecs/pix for the NIRC-2 and NACO detectors respectively.

The FWHMs of the experimental PSFs of the three filters of our 2002 observation is given in Table 2. In order to compare it with the theoretical FWHMs of Table 1, we plot the fractional differences of the experimental FWHM and the theoretical FWHM on Figure 3. Two things are notable here. The first is that the fractional regress gets smaller as we increase wavelength. This is because longer wavelengths are scattered less by the atmosphere, causing longer wavelength images to be closer to the ideal case. The second is that the fractional regress is small, the highest being 0.132 for the K_{cont} filter. This means that the stars follow the theoretical PSFs closely, signifying that the adaptive optics system we used, although imperfectly compensating for atmospheric turbulence, proved to be quite effective.

K_{cont} (arcseconds)	L' (arcseconds)	M_s (arcseconds)
$0.0797 \pm 5 \times 10^{-5}$	$0.134 \pm 5 \times 10^{-5}$	$0.155 \pm 5 \times 10^{-5}$

Table 2: The FWHMs of the experimental PSFs of our 2002 dataset. These values were calculated by fitting a gaussian on T Tau N of the final coadded images. Again, the errors are due to the uncertainties of the plate scale.

The FWHMs of the PSF of the 2006, 2008, and 2009 data is given in Table 3. Evidently, the 2008 and 2009 data possess FWHMs very close to that of the K_{cont} band of our 2002 dataset (the fractional standard deviation of the three FWHMs is a mere 0.057). This is because these datasets were taken with the same instrument (Keck's NIRC-2) with filters centered at very simillar wavelengths (the 2008 and 2009 datasets were taken with the $Br\gamma$ filter centered at 2.17 micron while the 2002 dataset's K_{cont} is centered

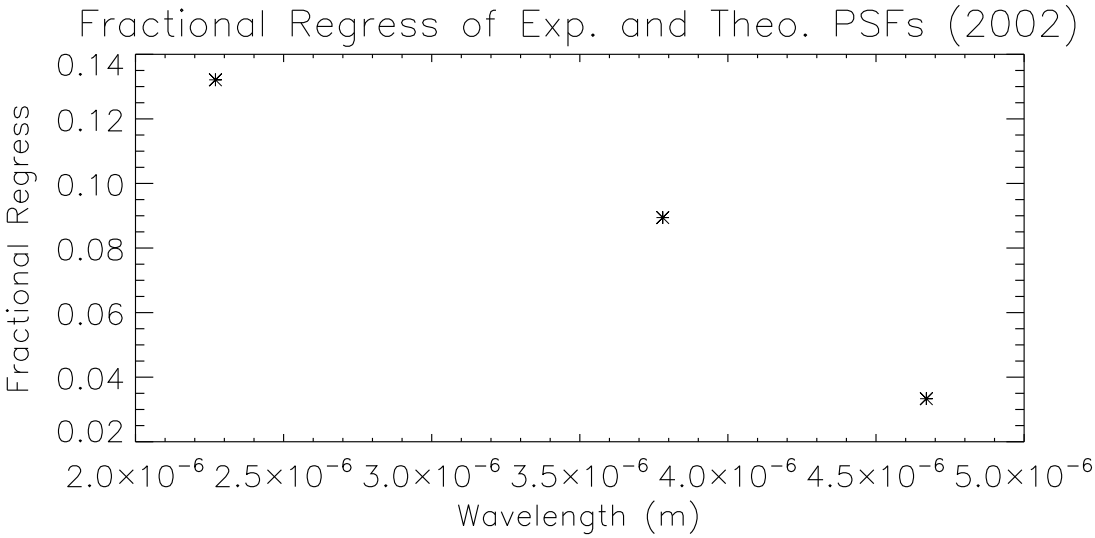

Figure 3: The fractional differences of the experimental FWHMs and the theoretical FWHMs versus wavelength of our 2002 observation. Note that the regress gets smaller as wavelength increases. This is because longer wavelengths are scattered less by the atmosphere, causing resolution of longer wavelength images to be closer to the ideal case.

at 2.27 micron). The slight differences of these three values stems from the fact that the 2008 and 2009 datasets were taken without the inscribed circle pupil method, thereby increasing the primary mirror diameter to almost 11 m along its longest side. Another reason for the differences is that the weather conditions might be different during the three observations. Although the Keck's adaptive optics system would try to compensate for the atmosphere, it is not perfect, therefore leaving different amounts of atmospheric blurrings affecting the PSFs of the different observations. The PSF of the 2006 observation varies greatly from the K_{cont} PSF of the 2002 observation (greater by a factor of 1.63) because the dataset was obtained using a completely different telescope. The VLT's 8.2 m diameter aperture, combined with the fact that the filter used, K_s was centered around 2.18 microns give its supposed theoretical best resolution (equation (1)) to be 0.0548 arcseconds. Therefore, our achieved resolution is 2.37 times lower than the best possible resolution.

2006 (arcseconds)	2008 (arcseconds)	2009 (arcseconds)
$0.130 \pm 6.6 \times 10^{-5}$	$0.0785 \pm 5 \times 10^{-5}$	$0.0716 \pm 5 \times 10^{-5}$

Table 3: The FWHMs of the experimental PSFs from our 2006, 2008, and 2009 datasets, calculated by fitting a gaussian to T Tau N. The errors here are due to the uncertainties in the plate scale.

3.4.3 Astrometry

In order to find the relative positions of the stars, first we construct gaussian fits on each of the stars using the method used in the previous section. The peaks of the gaussians would give us the approximate pixel location of each stars on our detector array. The pixel separations of each stars can then be calculated by finding the distances between each of the three points. We then convert this pixel distances to arcseconds by multiplying it with the plate scale of the camera ($0.01 \pm 5 \times 10^{-5}$ arcseconds/pixel). The uncertainties of this method would be the uncertainty associated with the gaussian (the standard deviation) and the uncertainty in the plate scale of the camera added in quadrature. In addition, a further uncertainty of 0.5 deg in absolute orientation also persist. This uncertainty does not factor into the distance calculations, but instead factors in the rotation of our images (the error of our North to the true North is 0.5 deg). An additional note is that for our

2002 dataset, we conduct astrometry only on the K_{cont} filter. This is done because the K_{cont} filter has the smallest wavelength, thus having the best possible resolution (as per equation (1)). The relative positions of each stars in each epochs relative to the position of T Tau Sa is given in Table 4. The distances between each stars, computed by taking the hypothenus differences of the coordinates in Table 4 are given in Table 5.

Obs. Year	Star	East of Sa (arcsecs)	North of Sa (arcsecs)	Uncertainties (arcsecs)
2002	N	0.140	0.673	0.0339
2002	Sb	-0.020	0.070	0.0339
2006	N	0.113	0.660	0.0554
2006	Sb	-0.013	0.050	0.0554
2008	N	0.119	0.661	0.0335
2008	Sb	-0.007	0.067	0.0335
2009	N	0.091	0.695	0.0305
2009	Sb	-0.005	0.070	0.0305

Table 4: The distances between each stars in our K_{cont} images of the 2002 observation.

Obs. Year	N to Sa (arcsecs)	N to Sb (arcsecs)	Sa to Sb (arcsecs)	Uncertainties (arcsecs
2002	0.687	0.623	0.072	0.0479
2006	0.670	0.622	0.052	0.0783
2008	0.672	0.607	0.067	0.0474
2009	0.701	0.632	0.07	0.0431

Table 5: The distances between each stars in our K_{cont} images of the 2002 observation. Note that for the VLT dataset, our uncertainty is larger than the Sa to Sb separation, therefore signaling that we had not corrected enough for the atmosphere to confidently distinguish them.

3.4.4 Photometry

In order to find the relative fluxes of T Tau Sa and T Tau Sb relative to T Tau N, we inscribe an aperture around the location of each stars found in the

preceeding section. We then find the total data number inside the aperture. We can then find the relative fluxes of T Tau Sa and T Tau Sb by dividing the maximum values inside their apertures with the maximum value inside an aperture inscribed within T Tau N. The radius used in this lab was judicially chosen to be 5 pixels. This radius was chosen because when doing aperture photometry of T Tau Sa and T Tau Sb, we need to conserve the radius of the aperture in order to prevent too much flux from T Tau Sa contaminating T Tau Sb and vice versa. By inspection, 5 pixel radius contained most of the fluxes of T Tau Sa and T Tau Sb at all epochs while still being conservative enough in keeping the least amount of flux contaminations from the other star. In effect, since we are doing relative photometry, this judicious choice would mostly cancel out due to us also applying the same aperture to T Tau N serving as reference star.

The uncertainty of this method comes from the Poisson noise added in quadrature with the sky noise. The Poisson noise is obtained by taking the square root of the total number of photon signals in the aperture (total data number multiplied by the gain), while the sky noise per pixel is gained by taking the standard deviation of the band's sky frame (or an empty patch of sky in the 2006, 2008, and 2009 datasets). The sky noise per pixel is then converted to total sky noise by multiplying it with the square root of the number of pixels in the aperture. When measuring the uncertainty of the fluxes of T Tau Sa and T Tau Sb relative to T Tau N, since all three fluxes have uncertainties, we would also need to use the error propagation equation[4] for an observable $I(F_1, F_2, ..., F_N)$:

$$\delta I = \sqrt{\left(\frac{\partial I}{\partial F_1}\delta F_1\right)^2 + ... + \left(\frac{\partial I}{\partial F_N}\delta F_N\right)^2} \tag{2}$$

The resulting relative fluxes of each stars on every band of our 2002 dataset are given in Table 6. The relative fluxes of each stars on the rest of the datasets are listed in Table 7.

[4]Taylor: An Introduction to Error Analysis

Filter	Sa	Sb
K_{cont}	0.0545 ±0.0017	0.091 ±0.0032
L'	0.307 ±0.0012	0.187 ±0.0011
M_s	0.490 ±0.0022	0.267 ±0.0017

Table 6: The relative fluxes of T Tau Sa and T Tau Sb with respect to T Tau N of our 2002 dataset.

Obs. Year	Sa	Sb
2006	0.0661 ±0.0053	0.0788 ±0.0062
2008	0.0539 ±0.0024	0.0522 ±0.0024
2009	0.118 ±0.0077	0.0724 ±0.0054

Table 7: The relative fluxes of T Tau Sa and T Tau Sb with respect to T Tau N of our 2006, 2008, and 2009 datasets.

3.5 Analysis

Using the known infrared wavelength magnitudes for T Tau N: 5.52, 4.32, 2.95 at K_{cont}, L', and M_s (all with uncertainties of $\pm 0.05 mag$), we can solve for the magnitudes of T Tau Sa and T Tau Sb at these wavelengths using the equation:

$$m_1 - m_2 = 2.5 * log \frac{f_2}{f_1} \tag{3}$$

Where m_1 and f_1 are the known magnitude and measured flux of T Tau N. The resulting magnitudes of T Tau Sa and T Tau Sb of our 2002 dataset is given in Table 8, where the uncertainties of the values in this table are solved using the error propagation equation (2).

Filter	Sa (mag)	Sb (mag)
K_{cont}	12.79 ±0.097	11.51 ±0.10
L'	7.28 ±0.060	8.51 ±0.057
M_s	4.73 ±0.066	6.25 ±0.066

Table 8: The magnitudes of T Tau Sa and T Tau Sb of our 2002 dataset.

If we plot $K - L'$ versus $K - M_s$ of these stars, we can put them on a color-color diagram shown in Figure 4. A pattern on this color-color diagrams obtained through numerous observations of known embedded protostars and T Tauri stars in the Taurus star-forming region is plotted in Figure 5. Comparing these two figures, we can see that T Tau N, T Tau Sa, and T Tau Sb lay on a line similar to that of Figure 5. Furthermore, following the classifications of Figure 5, evidently T Tau N is a T Tauri star with a disk, while T Tau Sa and T Tau Sb are embedded protostar. Furthermore we can also conclude, noting that older pre-mainsequence stars are located more to the bottom left than younger one, that T Tau N is the oldest of these three stars, followed by T Tau Sb, and then T Tau Sa.

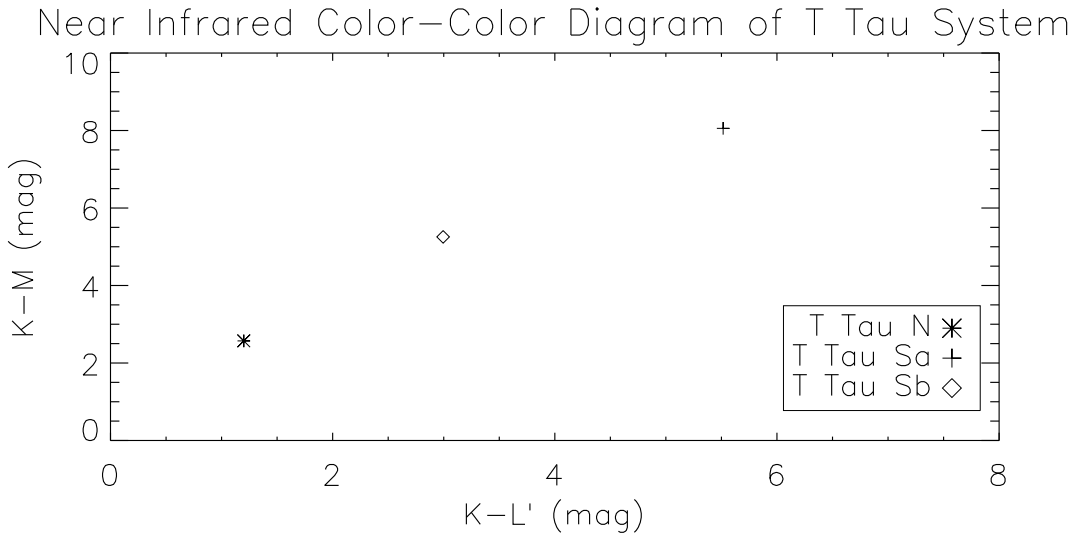

Figure 4: Color-color diagram of our 2002 dataset. Note that all of the points lay on a line simillar to that of Figure 5.

Assuming that the brightness of T Tau N does not vary significantly across our observation timelines, we can use equation (3) to solve for the magnitudes of T Tau Sa and T Tau Sb for the rest of our datasets. The results are given in Table 9. The plot of these magnitudes versus observation year is given in Figure 6. Evidently, T Tau Sa and T Tau Sb have magnitudes which vary with time. In fact, T Tau Sa was brighter than T Tau Sb until 2008, when the two magnitudes equalizes, and then proceed to be dimmer

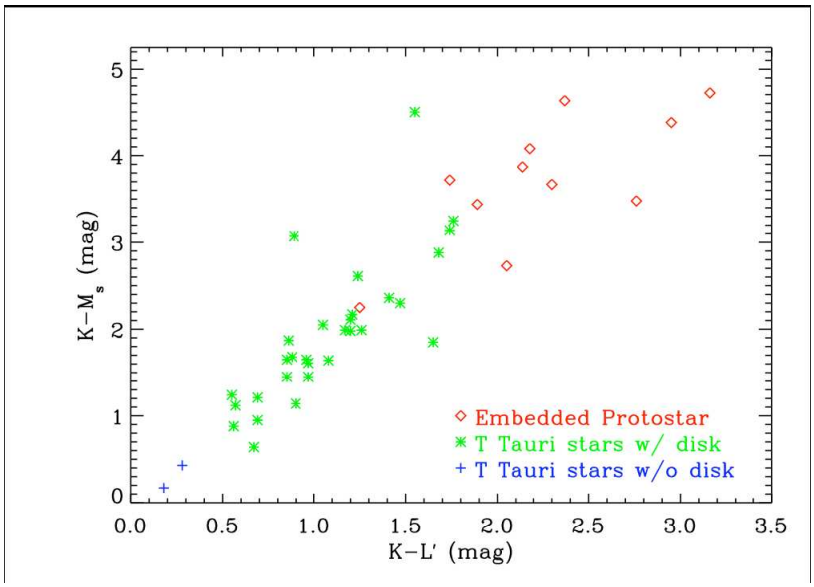

Figure 5: Color-color diagram of numerous other observations of known embedded protostars and T Tauri stars in the Taurus star-forming region, from the lab handout.

than T Tau Sb. This variability most probably stems from the fact that they have not reach main sequence yet (as from Figure 4). A protostar is highly variable because it had not found equilibrium between hydrogen fusion and gravitational contraction. Furthermore, shall one of these stars have a protoplanetary disk, clumps of materials orbiting around this disk can periodically transit over and dim the star.

Obs. Year	Sa (mag)	Sb (mag)
2006	12.3 ±0.28	11.9 ±0.27
2008	12.8 ±0.13	12.9 ±0.12
2009	10.9 ±0.083	12.1 ±0.075

Table 9: The magnitudes of T Tau Sa and T Tau Sb of our 2006, 2008, and 2009 datasets.

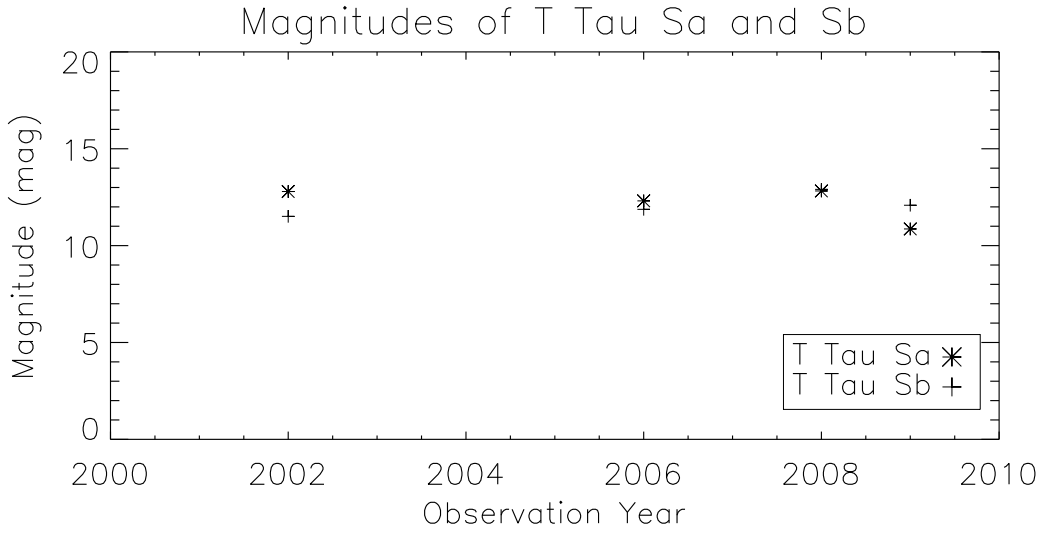

Figure 6: The magnitude of T Tau Sa and T Tau Sb of our 2006, 2008, and 2009 datasets plotted versus time. Note that their magnitude varies, and even switch positions before and after 2008. This means that they are variable stars.

4 Conclusion

In this lab, we have used adaptive optics in conjunction to NIRC-2 of Keck and NACO of VLT to peer into the T Tauri system in the near infrared. Using this method, we are able to confirm that the T Tauri system is composed of three pre-mainsequence stars. We were able to perform magnitude calculations for T Tau Sa and T Tau Sb, and confirm that they are indeed variable stars. In addition, we are able to calculate the separations between the three stars for every epochs. All of these details would be washed out by atmospheric turbulence, and making these measurements would be impossible without adaptive optics. Therefore, in essence, this lab had confirmed the capabilities and potentials of the adaptive optics system.

5 Appendix: Final Coadded Images

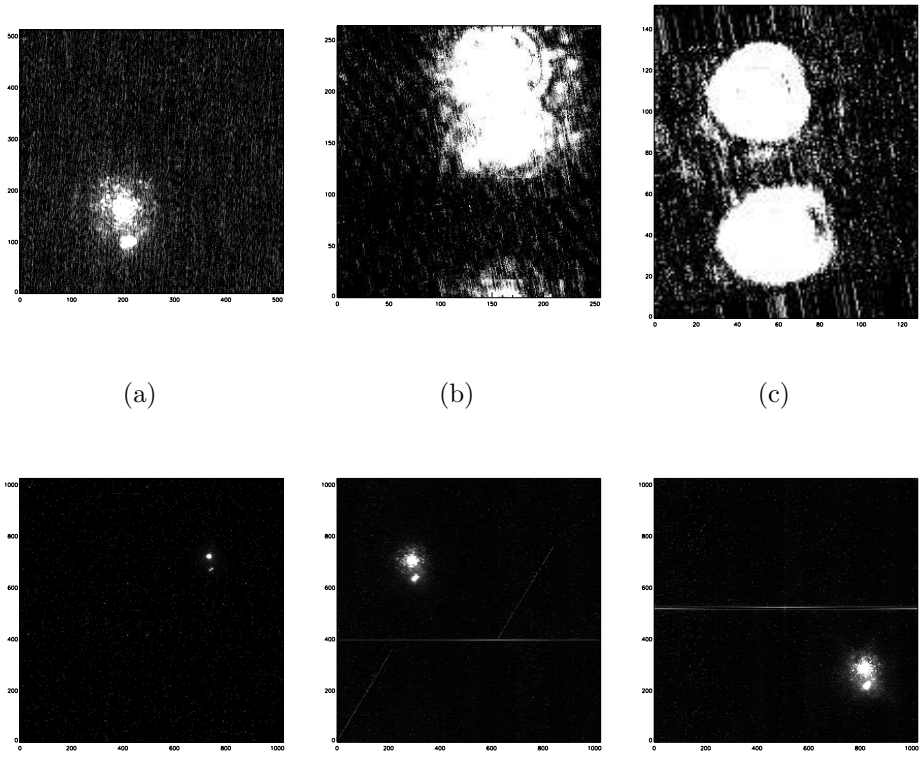

(a) (b) (c)

(d) (e) (f)

Figure 7: Final Coadded images of: a) 2002 K_{cont}, b) 2002 L', c) 2002 M_s, d) NACO's 2006, e) NIRC-2 2008, and f) NIRC-2 2009 datasets.